Reorganization of columnar architecture in the growing visual cortex

Wolfgang Keil[a,b,c], Karl-Friedrich Schmidt[d], Siegrid Löwel[d], and Matthias Kaschube[b,c,1]

[a]Max Planck Institute for Dynamics and Self-Organization, Göttingen 37073, Germany; [b]Lewis–Sigler Institute for Integrative Genomics, Princeton University, Princeton, NJ 08544; [c]Physics Department, Princeton University, Princeton, NJ 08544; and [d]Institute of General Zoology and Animal Physiology, Friedrich Schiller University, Jena 07743, Germany

Edited* by Charles F. Stevens, The Salk Institute for Biological Studies, La Jolla, CA, and approved May 25, 2010 (received for review November 17, 2009)

Many cortical areas increase in size considerably during postnatal development, progressively displacing neuronal cell bodies from each other. At present, little is known about how cortical growth affects the development of neuronal circuits. Here, in acute and chronic experiments, we study the layout of ocular dominance (OD) columns in cat primary visual cortex during a period of substantial postnatal growth. We find that despite a considerable size increase of primary visual cortext, the spacing between columns is largely preserved. In contrast, their spatial arrangement changes systematically over this period. Whereas in young animals columns are more band-like, layouts become more isotropic in mature animals. We propose a novel mechanism of growth-induced reorganization that is based on the "zigzag instability," a dynamical instability observed in several inanimate pattern forming systems. We argue that this mechanism is inherent to a wide class of models for the activity-dependent formation of OD columns. Analyzing one representative of this class, the Elastic Network model, we show that this mechanism can account for the preservation of column spacing and the specific mode of reorganization of OD columns that we observe. We conclude that column width is preserved by systematic reorganization of neuronal selectivities during cortical expansion and that this reorganization is well described by the zigzag instability. Our work suggests that cortical circuits may remain plastic for an extended period in development to facilitate the modification of neuronal circuits to adjust for cortical growth.

cortical growth | ocular dominance columns | postnatal development | critical period | zigzag instability

The brain of most mammalian species grows substantially during postnatal development without a significant change in the number of neurons. The human brain, for instance, weighs on average 350 g in newborns and 1,400 g in adult males (1). In cat, the neocortical volume increases from ≈1,000 mm^3 at birth to ≈4,500 mm^3 in adulthood (2). Consistently, the surface area of cat primary visual cortex (area 17 = V1) increases postnatally by a factor of 2.5 between week 1 and week 12 (3). This size increase implies that the distance between any two neuronal cell bodies grows on average by a factor of 1.6 during postnatal development. Do neuronal processes such as axons and dendrites simply elongate or are larger changes needed to accommodate this growth? It is not known at present how the brain achieves permanent adjustment of its functional wiring to the changing physical proportions while at the same time being fully functional at every moment. Whereas the importance of mechanical factors is appreciated in a number of growth-related phenomena in biology such as morphogenesis (4), heart development (5), and tumor growth (6), their possible impact on functional aspects of neural circuits has received relatively little attention.

In cat V1, much of the growth takes place during a period in which most parts of the visual field are already represented (7) and many neurons have already reached fairly mature levels of selectivity. For instance, the selective response of visual cortical neurons to inputs from one eye or the other, called ocular dominance (OD), can already be visualized at postnatal week 2 in cat V1 (8) (Fig. 1*A*). OD is organized into columns that can be labeled over the full extent of V1 as early as week 3 (9) (Fig. 1*B*). For these properties, this system is well suited for studying the impact of cortical growth on neural circuitry.

What happens to cortical columns when the cortex is growing in size? The seemingly simplest scenario, in which new columns are inserted into the cortex, appears rather implausible because the number of neurons remains largely constant during this period (10). In fact, most of the area increase is due to the generation of glial cells, the addition of more vasculature and connective tissue, and the myelinization of axons. To a lesser extent it also reflects the outgrowth and elaboration of axonal and dendritic processes (11). Therefore, a different scenario has been suggested, sometimes referred to as the "balloon effect," in which columns expand by a similar factor as the surrounding cortical tissue [see, e.g., (3)]. In this study, we start out by testing the balloon hypothesis for the case of OD columns in cat visual cortex. We show that the expected expansion of columns during cortical growth does not take place. Instead, columnar layouts reorganize over the considered period and become more isotropic in older animals. These observations strongly argue against a simple balloon-like expansion and imply that cortical circuits can respond to the constraints arising during growth by a different as yet unknown mechanism.

In order to account for our empirical observations, a fraction of neurons must either shift their relative spatial location or, alternatively, alter their functional response properties. Although appealing, the former possibility is difficult to address at present, because little is known about coherent motion of groups of neurons in response to mechanical tension (12–14). In contrast, a large body of experimental and theoretical work exists addressing phenomena related to cortical plasticity and demonstrating the impressive susceptibility of neural circuits to changes in activity patterns, frequently in the context of OD (15, 16). Furthermore, it is noteworthy that in the two most intensely studied animal models for cortical plasticity, namely the cat and the mouse, the period of brain and body growth coincide with and end at about the same time as the period that allows for intense restructuring of neuronal connections (17–19). In this study, we therefore explore the latter possibility and analyze the predicted reorganization in models for the activity-dependent formation of OD columns. Based on general properties of these models, we develop a scenario of growth-induced cortical reorganization. Characteristic features of this reorganization as well as the time scale on which it evolves are in good agreement with the changes in columnar layout we observe during postnatal growth in cat V1.

Author contributions: W.K., S.L., and M.K. designed research; W.K., K.-F.S., S.L., and M.K. performed research; W.K. and M.K. analyzed data; and W.K., S.L., and M.K. wrote the paper.

The authors declare no conflict of interest.

*This Direct Submission article had a prearranged editor.

[1]To whom correspondence should be addressed. E-mail: kaschube@princeton.edu.

This article contains supporting information online at www.pnas.org/lookup/suppl/doi:10.1073/pnas.0913020107/-/DCSupplemental.

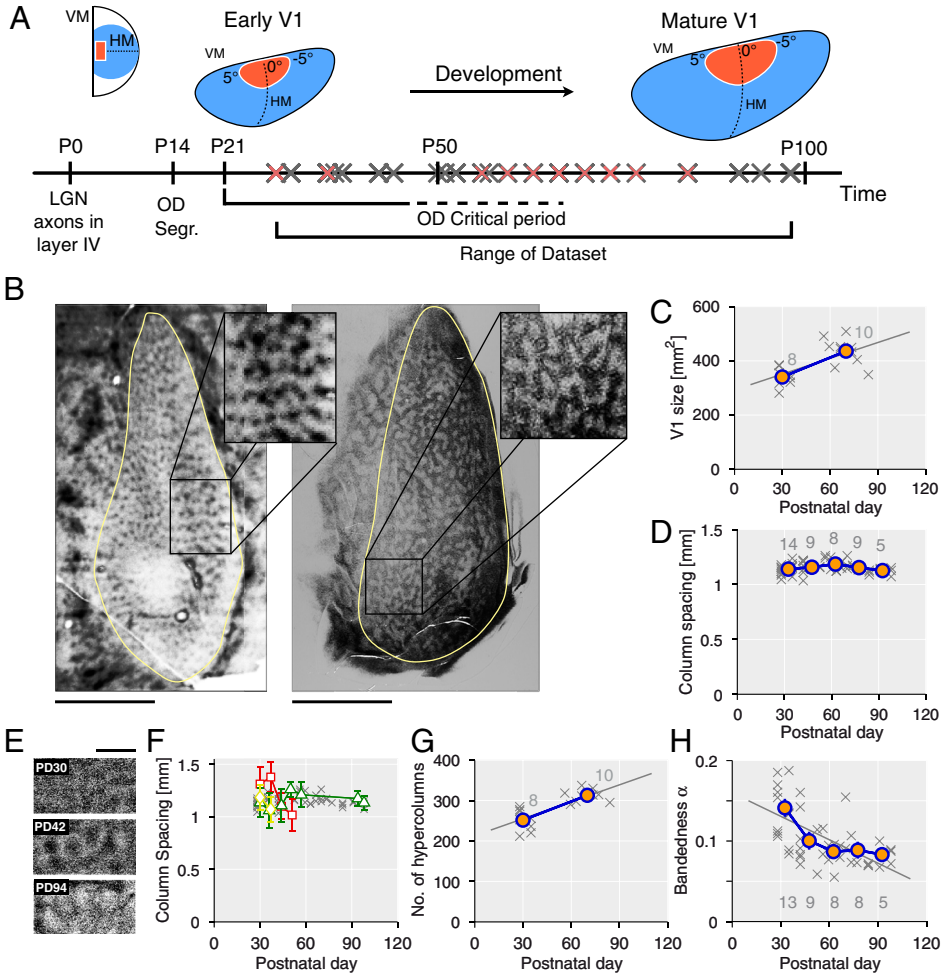

Fig. 1. Reorganization of OD columns in cat V1 over a period of cortical growth. (*A*) Growth of cat V1, the representation of the visual hemifield (blue area, V1; red area, central visual field representation; HM, horizontal meridian; VM, vertical meridian), and the time line of cat OD development. Our dataset includes 2-DG/proline-labeled hemispheres from kittens between PD28 and PD98 (2-DG, $N = 37$; proline, $N = 4$) and chronic optical recordings between PD30 and PD98 (crosses mark individual data points). (*B*) Two representative examples of OD layouts. Left, at PD30 (2-DG); right, at PD60 (proline). Yellow lines mark V1 borders (scale bar, 10 mm). (*C*) Area sizes of V1 for the $N = 18$ kittens with complete reconstructions of V1 (red-marked crosses in *A*). Blue-orange dots represent averages over pools of sizes denoted by the gray numbers. Gray crosses mark values for individual animals. Gray line shows linear regression ($r = 0.62$, $p < 0.006$). (*D*) OD column spacings Λ do not increase over this period ($r = -0.034$, $p < 0.83$). (*E*) OD columns in cat V1 by intrinsic signal optical imaging [same animal; high-pass filtered (*SI Appendix*); scale bar, 1.5 mm]. (*F*) Column spacings Λ for the case in (*E*) (green triangles; error bars by bootstrapping) and for two other cases (red boxes, yellow diamonds) corroborating the results in (*D*) (shown in light gray for comparison). (*G* and *H*) Whereas the number of hypercolumns N_{HC} increases over this period (*G*) ($r = 0.77$, $p < 0.0002$), the bandedness α decreases considerably (*H*) ($r = -0.58$, $p < 6 \cdot 10^{-5}$). Note that error bars for pool averages in *C*, *D*, *G*, and *H* are smaller than the symbol size.

Results

The Spacing of OD Columns Is Preserved Over a Period of Cortical Growth. We first measured the size increase of cat V1 during early postnatal development (Fig. 1*A*). We labeled complete layouts of OD columns in V1 visualized by either 2-[^{14}C]-deoxyglucose (2-DG) or [^{3}H]-proline in kittens at different ages between postnatal day (PD) 28 and PD98 ($N = 18$ hemispheres, Fig. 1*B*). V1 is readily discernible by its distinctive columnar activation pattern in comparison to the labeling in surrounding cortical areas (20). In particular, V1 is distinguished from the secondary visual cortex (area 18 = V2) based on its considerably smaller column spacing. We observed a size increase of about a factor of 1.3 between two groups centered at PD30 and PD70 ($r = 0.62$, $p < 0.006$) (Fig. 1*C*). To reduce possible influences of genetic variability (21), we analyzed a littermate couple on PD30 and PD72. Consistent with our previous results, V1 area is a factor of 1.46 larger in the older kitten. Thus, our analyses confirm previous studies (3, 9) by observing a considerable size increase of V1 during cat postnatal development.

We next asked whether the spacing of OD columns increases by a corresponding factor over this period. First, we measured the column spacing Λ of 2-DG/proline-labeled OD patterns in $N = 41$ hemispheres between PD28 and PD98 (data includes the $N = 18$ hemispheres used for the analyses of V1 sizes). To obtain accurate estimations of column spacings, we used the wavelet method introduced in (21, 20) (*SI Appendix*). As shown in Fig. 1*D*, column spacings vary between 1.05 mm and 1.28 mm, but do not show a significant increase over this period ($r = -0.034$, $p < 0.83$). Consistent with this observation, the column spacings of the two littermates differ by <10%, despite their difference in V1 size of 46%.

To follow the development of column spacings in individual hemispheres, we visualized OD columns by chronic optical imaging ($N = 3$ hemispheres; total age range PD30–PD98) (Fig. 1*E*). We quantified their spacings by the above wavelet method (Fig. 1*F*). Whereas column spacings based on optical recordings exhibit larger variability compared to the 2DG/proline data (Fig. 1*F*), we found no systematic increase of column spacings in individual animals, thus confirming the conclusions drawn from the 2DG/proline data. Increased variability might be explained by the substantial intraareal variability of OD column spacings (20) together with the fact that the imaged regions were much smaller than V1 and may have shifted with age.

Taken together, both the 2-DG/proline data and the chronic optical recordings demonstrate that the postnatal growth of cat V1 is not accompanied by a corresponding increase in the spacing of OD columns, strongly arguing against the balloon scenario.

OD Columns Reorganize During Cortical Growth. An increase of area without a change in column spacing indicates an increase in the number of hypercolumns. The concept of a hypercolumn is related to that of a functional module and denotes a cortical unit containing a full set of values for any given set of receptive field parameters (22). We roughly estimated the typical size of a hypercolumn by Λ^2 (*SI Appendix*) and defined the number of hypercolumns in a map by $N_{HC} = A/\Lambda^2$ (20), where A is its total area. Fig. 1*G* shows that for the $N = 18$ completely reconstructed hemispheres from Fig. 1*C* the number of hypercolumns N_{HC} increases significantly ($r = 0.77, p < 0.0002$). At PD28, V1 contains

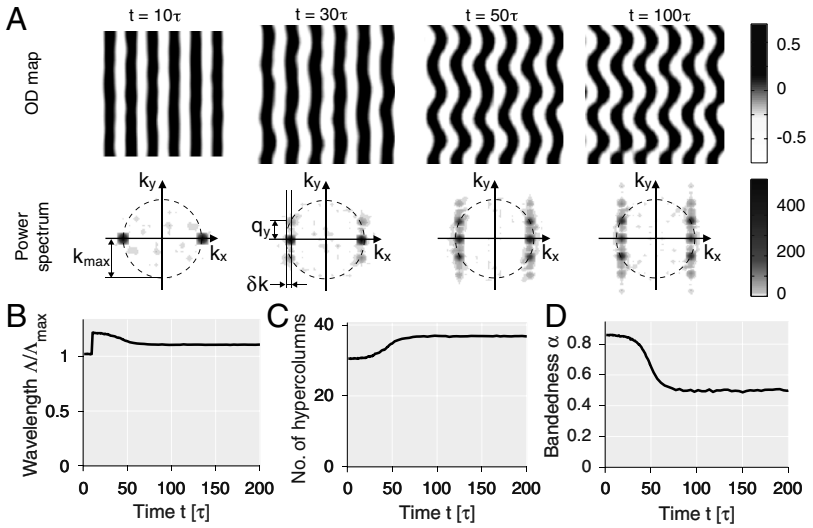

Fig. 2. Expansion-induced reorganization in models for OD formation. (*A*) Snapshots of a simulation of the EN model (23) starting from a near steady state solution; i.e., a stripe-like OD pattern (upper row) corresponding to a single Fourier mode in the power spectrum (lower row) ($\eta = 0.025$, $r = 0.15$). After instantaneous area increase (linear extent by a factor of 1.18; i.e., $\delta k/k_{max} = -0.15$; at 10τ), OD domains bend sinusoidally and additional Fourier modes appear at $\approx(k_{max} + \delta k)\vec{\mathbf{x}} \pm q_y\vec{\mathbf{y}}$. (*B–D*) This reorganization is captured by the column spacing Λ (*B*), the number of hypercolumns N_{HC} (*C*), and the bandedness α (*D*) (time in units of the time scale τ of OD segregation).

on average 260 ± 40 hypercolumns ($N = 5$), increasing to 319 ± 17 ($N = 6$) at PD72 (increase of 23%).

To reveal more directly the reorganization of OD columns, we analyzed a third parameter called bandedness α that characterizes the structural properties of local pattern elements (21, 20) (Fig. S1). Large values of α indicate layouts composed of regular stripe-like parallel domains, whereas small values indicate more isotropic layouts such as bended stripes or patches. Such quantitative evaluation of the spatial organization of columns was possible in $N = 39$ hemispheres. We found that the bandedness α decreases by almost a factor of 2 from an average of 0.14 ± 0.02 ($N = 13$) at PD35 to an average of 0.083 ± 0.006 at PD95 ($N = 5$) ($r = -0.58$, $p < 6 \cdot 10^{-5}$) (Fig. 1*H*). This systematic decrease in bandedness indicates that OD columns, while largely preserving their initial spacing, reorganize and develop more isotropic layouts over time.

Modeling OD Column Formation with Growth. To understand these experimental observations, we studied cortical growth in models for the activity-dependent self-organization of OD columns. For specificity, we focussed on the well-studied Elastic Network (EN) model (23–25) (*Materials and Methods* and *SI Appendix*). Solutions in the absence of growth are shown in Fig. S2 and Movie S1. Linear stability analysis around the initially nonselective cortex (ref. 24 and *SI Appendix*) identifies a control parameter r describing the distance from the pattern formation instability threshold. A pattern of OD columns forms for $r > 0$. The analysis also defines an intrinsic timescale $\tau = 1/r$, on which the segregation of columns takes place, and a spatial scale Λ_{max} that is roughly equal to the column spacing of the developing OD pattern. As in other models for the self-organization of OD columns (25–28), this spatial scale arises from the effective recurrent interactions that have a "Mexican-hat" structure (local facilitation, nonlocal suppression). In agreement with previous work (24, 25), we find in simulations that an OD pattern emerges after a few τ (Fig. S2 and Movie S1). The only steady state solutions we observe are parallel OD stripes.

As a simple way to mimic cortical growth, we started from steady state solutions and abruptly increased isotropically the size of the simulated system without changing the other model parameters (i.e., without increasing the width of the Mexican-hat) (*Materials and Methods* and *SI Appendix*). Fig. 2 displays snapshots of a typical example of such a simulation (see also Movie S2). Upon size increase at $t = 10\tau$, stripes start to bend sinusoidally (Fig. 2*A*, upper row). In the power spectrum, this corresponds to the growth of new Fourier modes on both sides of the original mode of the stripe pattern (Fig. 2*A*, lower row).

We quantitatively analyzed this reorganization by the wavelet method used above. The column spacing Λ increases abruptly at 10τ, but subsequently decreases to close its initial value (Fig. 2*B*). The number of hypercolumns N_{HC} increases persistently (Fig. 2*C*), whereas the bandedness α decreases significantly over this period (Fig. 2*D*). Thus, the growth-induced bending of OD columns largely restores the initial spacing and results in a bandedness drop similar to what we observe in experiment (Fig. 1).

A General Mechanism of Growth-Induced Reorganization. We argue that this type of expansion-induced reorganization of OD columns in the EN model is caused by a zigzag (ZZ) instability (29), a type of dynamical instability that has been widely studied in the theory of pattern formation (30, 31). Fig. 3 *A* and *B*. This instability is typical for the wide class of relaxational, rotationally symmetric models in which a two-dimensional pattern forms by a finite wavelength instability (30). This class includes the EN model, as we outline in the *SI Appendix*, and many other OD models (e.g., refs. 25–28).

A theory (31, 32) for this model class exists predicting the regime of the ZZ instability (Fig. 3*C*, *Inset*). However, strictly speaking, this theory is valid only in a narrow parameter region close to the point of instability threshold at $r = 0$. We therefore analyzed numerically the behavior of the EN model further away from threshold by probing systematically a large set of instantaneous size increases and testing for growing ZZ modes (Fig. S3 and *SI Appendix*). We observed that the regime of ZZ instability is very large (Fig. 3*C*). Similar to the theoretical predictions (31, 32), even a slight expansion results in a ZZ instability and its regime increases parabolically with the control parameter r. Moreover, the induced reorganization evolves on a time scale τ_{ZZ} that for small expansions exceeds the time scale τ of OD column segregation by more than an order of magnitude.

Realistic Growth Scenarios. Finally, we show that growth-induced reorganization shows signatures of the ZZ instability even if the initial OD layout is not a simple stripe pattern and the increase in system size follows a continuous growth scenario. To approximate realistic conditions, we initialized our simulations with the nonselective state and linearly increased the linear extent of the simulated regions by a factor of 1.6 (factor of 2.56 in area increase) between $t = 0\tau$ and $t = 100\tau$. Fig. 4*A* shows that layouts appear to be more bended in a ZZ-fashion when compared to simulations for which we stopped growth after $t = 10\tau$. Typically, the column spacing Λ in growing systems increases only transiently (Fig. 4*B*) implying that the hypercolumn number N_{HC} increases persistently (Fig. 4*C*). The bandedness α is relatively

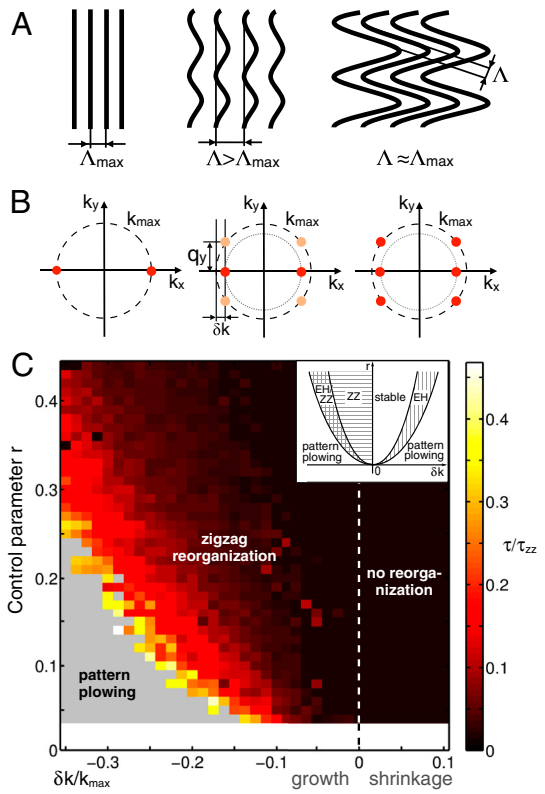

Fig. 3. The ZZ instability provides a general framework for understanding growth-induced cortical reorganization. (*A*) The ZZ mechanism: Initially, OD stripes exhibit the spacing Λ_{max} (*Left*). Upon expansion (*Center*), OD stripes recover their initial spacing locally through bending of OD stripes (*Right*). (*B*) In Fourier space: Two new Fourier modes grow at $(k_{max}+\delta k)\vec{x} \pm q_y\vec{y}$ restoring the initial wave number k_{max} of the pattern. (*C*) Regime and time scale of ZZ instability in the EN model. Instantaneous isotropic expansion (regime left of white dashed line) induces a ZZ reorganization that evolves on a timescale $\tau_{ZZ} \gg \tau$ (*SI Appendix*). For very large expansion (gray region), a complete new pattern forms (pattern plowing). For area decrease (right of white dashed line) no reorganization was observed. No simulations were carried out in the white region, because the simulation time diverges for $r \to 0$ (*SI Appendix*). (*Inset*) Predicted regime of ZZ instability for two-dimensional, relaxational, isotropic dynamics close to instability threshold ($r \ll 1$) [redrawn from (31); horizontally striped region, ZZ instability; vertically striped region, Eckhaus (EH), instability; i.e., insertion/elimination of a stripe (*SI Appendix*)].

variable across solutions reflecting the large diversity of the evolving OD layouts (Fig. 4*D* and Fig. S2). However, whereas in virtually all simulations without growth α increases nearly monotonically (Fig. S2 and Movie S1), in growing systems α typically drops considerably reflecting the ZZ-type reorganization of OD columns (Fig. 4*A* and Movie S3).

We systematically studied the growth-induced reorganization by varying the control parameter r and testing different area increases (factor of 1, 1.44, 1.96, 2.56, and 3.24, Fig. 4 *F–H* and *SI Appendix*). We measured the difference $\Delta\alpha$ between the first maximum in bandedness and the subsequent minimum and the time interval Δt between these two bandedness extrema [Fig. 4*E*, based on eighth-order polynomial least square fit (*SI Appendix*)]. Whereas drops with $\Delta\alpha > 0.05$ and $\Delta t > 15\tau$ occurred in only <6% of the nongrowing systems, already with moderate growth, they are present in a large fraction of systems (Fig. 4*F*). For smaller values of r the drop is generally more pronounced. Both the average size $\Delta\alpha$ and the duration Δt depend only weakly on the total area increase and drops last on average $>40\tau$ (Fig. 4 *G* and *H*).

Thus, also for more realistic growth scenarios, the induced reorganization exhibits key features of a ZZ instability, in particular the only mild and transient increase in column spacing and the prominent and long lasting drop in bandedness. Intriguingly, these features also describe the mode of reorganization we observe in experiment (Fig. 1). Moreover, if we identify the model time unit τ with roughly 1 d in cat postnatal development—an assumption that may be justified by experiments showing that OD columns segregate within a few days (e.g., ref. 8)—we observe that even the time scales on which these changes evolve, agree fairly well between model and experiment. This suggests that the reorganization we observe in experiments is caused by cortical expansion through a mechanism that is based on the ZZ instability.

Discussion

Cortical Expansion, the Absence of the Balloon Effect and the Range of the Mexican Hat. Our empirical data provides evidence against the so-called balloon effect (3) by showing that OD columns do not simply expand during cortical growth, but largely maintain their spacing. At first sight, a balloon-like expansion may seem plausible. For instance, in vitro connected neurons, when moderately pulled apart, readily extend their axonal arbors to prevent disruption, thereby achieving neurite growth rates of up to 1 cm/day (13). However, mechanical tension on one axonal branch can strongly influence the arborization of other branches of the same neuron (14), indicating that expansion-induced responses can be rich and may lead to nontrivial collective behavior in expanding networks of interconnected neurons.

Models for the activity-dependent formation of OD columns can reproduce the absence of the balloon effect if the width of the lateral interactions is kept fixed during growth as we assume in this study. In the EN model, an effective intracortical interaction of Mexican-hat type (Fig. S2*A*) arises from the interplay between the coactivation of cortical regions and a tendency for neighboring neurons to acquire similar response properties (23). Even if the interaction range increases by only half the rate of the cortex, we observe a ZZ-type reorganization accompanied by a bandedness drop (*SI Appendix* and Fig. S8). However, in this case also the column spacing increases systematically. Thus, these models can be reconciled with our data only if the interaction range does increase only little during growth.

There are several possibilities of why the range of effective lateral interactions might not increase during growth. It is conceivable that the width of interaction could depend on the lateral spread of dendritic arbors. Limits on an increase of the arbor size during growth might be imposed by a tendency of neuronal circuits to minimize the total length of wiring (e.g., ref. 32) and could be achieved by synaptic pruning (10). Alternatively, interactions of Mexican-hat type could arise if the time scales of the dominant inhibitory synapses are small compared to excitatory synapses (33). Thus, a possible shift from a dominance of smaller toward larger synaptic timescales during the period of growth could partly compensate for the increase of the distance between neurons. Finally, Mexican-hat type interactions could arise by excitatory connections that at larger distances preferentially target inhibitory interneurons. In this case, the width of interactions may depend on the strength of inhibition (16), which, appropriately adjusted, could keep the range of the Mexican-hat constant during growth.

Reorganization vs. Displacement. In the scenario of growth-induced reorganization proposed in this paper, increasing distances between cell bodies alter the effective lateral interactions between neurons, thereby inducing shifts in the response properties in a fraction of them. Alternatively, one may explore a scenario in which neuronal response properties are preserved, and the mature columnar layout is obtained by an inhomogeneous displacement of cells. Strong intracolumnar connections may provide the necessary mechanical stability for keeping cells within columns closer to one another. However, the ability of neurons to rapidly

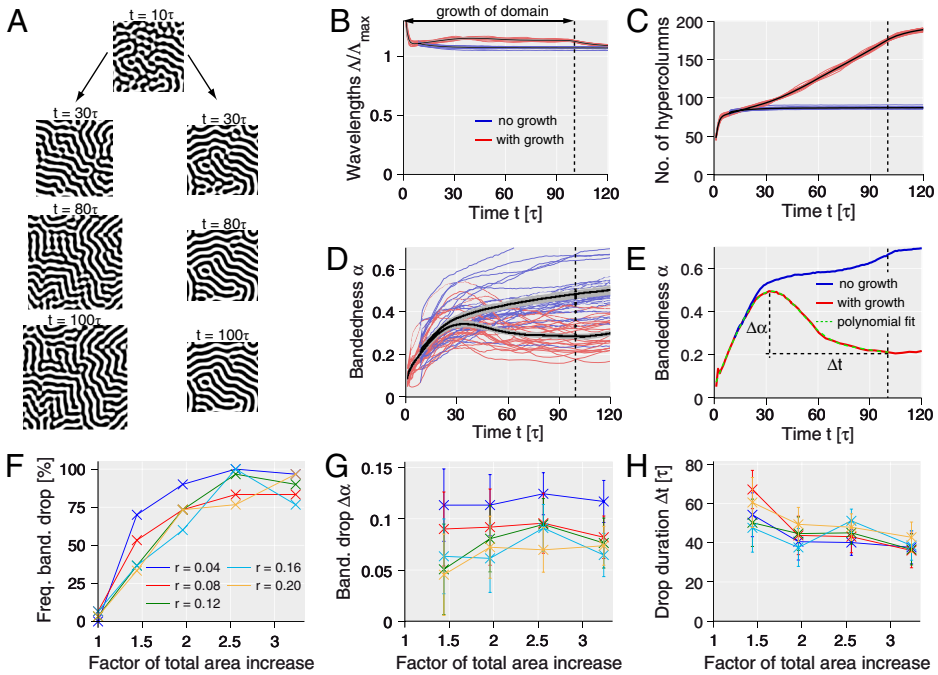

Fig. 4. ZZ-type reorganization of OD columns in a realistic growth scenario. (*A*) Snapshots of EN model simulations with isotropic linear area increase by a factor of 2.56 between $t = 0$ and $t = 100\tau$ (left column) and without size increase after $t = 10\tau$ (right column) ($r = 0.16$, $\eta = 0.025$). (*B–D*) Time courses of column spacing Λ (*B*), number of hypercolumns N_{HC} (*C*), and bandedness α (*D*) for 30 pairs of simulations as in *A*. Black curves are averages, gray regions SEM. Despite the large area increase, growing systems display an only mild and transient increase in Λ implying a strong increase in N_{HC}, while α typically drops considerably. (*E*) Quantification of bandedness drop by its strength $\Delta\alpha$ and duration Δt. (*F–H*) The percentage of simulations showing a substantial bandedness drop (defined by $\Delta\alpha > 0.05$, $\Delta t > 15\tau$) (*F*), the average size $\Delta\alpha$ of such drops (*G*) and their average duration Δt (*H*) evaluated for various total area increases and control parameters r ($N = 50$ simulations per data point, error bars indicate SEM).

extend their axonal arbors in response to mechanical tension (13) raises doubts about expansion-induced forces being strong enough to promote inhomogeneous displacement of cells. Following the spatial positions as well as functional response properties of many cells experimentally (e.g., by chronic 2-photon microscopy) could help to disentangle these two hypotheses. Moreover, experiments that, instead of altering the patterns of neural activity, measure and/or apply mechanical stress to cortical tissue or individual neuronal processes in vivo may reveal further insights into the role of mechanical tension in cortical development. A better understanding of the interplay between tension-mediated and activity-driven mechanisms in shaping neural circuits in vivo could shed new light on normal development and cortical growth, but potentially also on the response of neural network function to cortical lesions and brain tumors.

The two scenarios have different implications for the hypercolumn as a functional cortical unit. A shift in OD in individual neurons would alter the set of stimulus representations in a hypercolumn. It would be interesting to monitor simultaneously other neuronal selectivities and test whether they codevelop in a systematic fashion; e.g., by improving coverage uniformity (34) over time. On the other hand, a pure displacement of groups of neurons would distort the original hypercolumn and result in systematic inhomogeneities in the cortical representation of the visual field position. Such inhomogeneities may be detectable in the mature cortex even without the necessity of technically very challenging chronic experiments.

Relation to Previous Work. A longitudinal optical imaging study (35) of OD columns in a single strabismic cat reported an increase of OD column spacing between PD27 and PD61 consistent with the slight but not significant increase we observe over this period (Fig. 1*D*). A chronic imaging study in ferret reported a fairly stable spatial organization of orientation columns between PD30 and PD55 (36). However, a more recent study (37) analyzing orientation columns in the cat between PD35 and PD105 observed changes in local column spacing that were coordinated between V1 and V2. Consistent with the present study, the average spacings in V1 and V2 remained largely constant over this period. A theoretical study (38) of a one-dimensional model of OD development during cortical growth predicts a splitting of OD stripes analogous to the Eckhaus instability (*SI Appendix*). As we show here, two-dimensional models exhibit a much richer dynamics and behave qualitatively differently.

A Novel Function of Plasticity in Normal Development. The impressive ability of cortical circuits to reorganize during and after the critical period has been demonstrated in numerous studies by artificially manipulating cortical activity; e.g., by monocular deprivation (see ref. 16 for a review). However, relatively little is known at present about the role of cortical plasticity for normal cortical development (8, 15), but see refs. 37, 39. As we point out in this study, the period of cortical plasticity in cat visual cortex overlaps with the period of postnatal cortical growth (17). Whereas the peak of the classical critical period is around PD30 (40), cortical plasticity does not cease after the critical period, but rather declines gradually (16). It is readily conceivable that this plasticity may be exploited by the cortex to accommodate for growth-induced changes. Interestingly, the reorganization we report here is largest close to the peak of the critical period. (Fig. 1*H*). Furthermore, key features of this reorganization are reproduced by modeling OD formation as self-organization based on cortical plasticity. Thus, we conclude that cortical plasticity may play an important role in normal development through facilitating growth-related modifications of neuronal circuits.

Materials and Methods

Experiment. OD patterns were labeled with 2-[^{14}C]-deoxyglucose (2-DG) autoradiography after monocular stimulation of the animals or by [^{3}H]-proline autoradiography after injection of the labeled proline into one eye that labels the thalamocortical afferents of that eye in cortical layer IV

(see ref. 20 and therein). OD columns were recorded by intrinsic signal optical imaging following ref. 41.

Model. OD is described by a real valued field $o(\mathbf{x},t)$, where $\mathbf{x}$ represents the position on the cortical surface and t time. Negative/positive values of $o(\mathbf{x},t)$ indicate a preference for inputs from the ipsilateral/contralateral eye. The dynamics of this field is given by

$$\partial_t o(\mathbf{x},t) = \langle [s_o - o(\mathbf{x},t)] A_\sigma(\mathbf{x},\mathbf{S},o(\cdot\,,t)) \rangle_{\mathbf{S}} + \eta \Delta o(\mathbf{x},t), \qquad [1]$$

where

$$A_\sigma(\mathbf{x},\mathbf{S},o(\cdot\,,t)) = \frac{e^{-(|\mathbf{s}_r-\mathbf{x}|^2+|s_o-o(\mathbf{x},t)|^2)/2\sigma^2}}{\int d^2y e^{-(|\mathbf{s}_r-\mathbf{y}|^2+|s_o-o(\mathbf{y},t)|^2)/2\sigma^2}}$$

is the cortical activity pattern, σ controls the receptive field size in the stimulus parameter space, $\langle\cdot\rangle$ denotes the average of the ensemble of visual stimuli $\{\mathbf{S}\}$, η measures the strength of lateral interactions and Δ is the two-dimensional Laplacian. Visual stimuli $\mathbf{S} = (\mathbf{s}_r, s_o)$ are point-like and characterized by a location $\mathbf{s}_r$ and an OD value s_0, which describes whether the activated units are forced to prefer the ipsilateral ($s_o < 0$) or the contralateral ($s_o > 0$) eye.

Numerical Integration. Simulations were performed on a 64×64 grid with periodic boundary conditions. We used at least 4 grid points per $\Lambda_{\max}$ and an integration time step $\delta t = \min\{1/(20\eta k_{\max}^2), \tau/10\}$. The first term on the right hand side of Eq. **1** was treated by an Adams–Bashforth scheme, the second term by spectral integration. $\mathbf{s}_r$ and s_o were uniformly distributed with $\langle s_o^2 \rangle = 1$. Typically, between 4×10^4 and 2×10^5 stimuli were used per integration step.

Instantaneous Area Increases. We rescaled the system length L as determined from the desired value of $\delta k/k_{\max}$ (no change in number of grid points; see *SI Appendix*). We adjusted the number of stimuli, N_s, and, because $\Delta \sim 1/L^2$, the matrix for the spectral integration step. The numerical value of σ remained constant.

Continuous Area Increases. We linearly increased the linear extent L of the simulated regions between $t = 0\tau$ and $t = 100\tau$ and updated the Laplacian Δ and the number of stimuli N_s at every integration step.

Data Analysis Method. Column spacing Λ and bandedness α of both data and simulations, were analyzed using the wavelet method introduced in ref. 21. An overcomplete basis of complex Morlet wavelets at various scales and orientations was compared to the OD pattern at each spatial location. Λ was estimated by the scale of the best matching wavelet, α by the angular variance of matching at that scale (*SI Appendix*).

Statistics. r-values denote Pearson's linear correlation coefficient; p-values were obtained with Student's t tests.

All methods are described in detail in the *SI Appendix*.

ACKNOWLEDGMENTS. We thank F. Wolf for many inspiring discussions, and M. Huang and M. Schnabel for help with numerical procedures. We thank S. Palmer and P. Mehta for helpful comments on the manuscript. W. K. and M. K. acknowledge financial support from Grant 01GQ0430 from the German Ministry for Education and Science (BMBF) via the Bernstein Center for Computational Neuroscience (BCCN), Göttingen. M.K. was supported by Grant P50 GM071508 from the National Institute of Health and the National Institute of General Medical Sciences. K.-F. S. and S. L. acknowledge financial support from BMBF Grants 01GQ07111 and 01GQ0921.

1. Dekaban AS, Sadowksy D (1978) Changes in brain weight during the span of a human life: Relation of brain weight to body heights and body weights. *Ann Neurol* 4:345–356.
2. Villabanca JR, Schmanke TD, Crutcher HA, Sung AC, Tavabi K (2000) The growth of the feline brain from fetal into adult life I. A morphometric study of neocortex and white matter. *Dev Brain Res* 122:11–20.
3. Duffy KR, Murphy KM, Jones DG (1998) Analysis of the postnatal growth of visual cortex. *Vis Neurosci* 15:831–839.
4. Martin AC, Gelbart M, Fernandez-Gonzalez R, Kaschube M, Wieschaus EF (2010) Integration of contractile forces during tissue invagination. *J Cell Biol* 188:735–749.
5. Vermot J, et al. (2009) Reversing blood flows act through klf2a to ensure normal valvulogenesis in the developing heart. *PLoS Biol* 7:e1000246.
6. Kumar S, Weaver VM (2009) Mechanics, malignancy, and metastasis: The force journey of a tumor cell. *Cancer Metastasis Rev* 28:113–127.
7. Sireteanu R, Maurer D (1982) The development of the kitten's visual field. *Vision Res* 22:1105–1111.
8. Crair MC, Horton JC, Antonini A, Stryker MP (2001) Emergence of ocular domi nance columns in cat visual cortex by 2 weeks of age. *J Comp Neurol* 430:235–249.
9. Rathjen S, Schmidt KE, Löwel S (2003) Postnatal growth and column spacing in cat primary visual cortex. *Exp Brain Res* 149:151–158.
10. Cragg BG (1975) The development of synapses in the visual system of the cat. *J Comp Neurol* 160:147–166.
11. Purves D (1994) *Neural activity and the growth of the brain* (Cambridge University Press, Cambridge, UK).
12. van Essen DC (1997) A tension based theory of morphogenesis and compact wiring in the central nervous system. *Nature* 385:313–318.
13. Smith DH (2009) Stretch growth of integrated axons tracts: Extremes and exploitations. *Prog Neurobiol* 89:231–39.
14. Anava S, Greenbaum A, Jacob EB, Hanein Y, Ayali A (2009) The regulative role of neurite mechanical tension in network development. *Biophys J* 96:1661–1670.
15. Katz L, Crowley J (2002) Development of cortical circuits: Lessons from ocular dominance columns. *Nat Rev Neurosci* 3:34–42.
16. Hensch TK (2005) Critical period plasticity in local cortical circuits. *Nat Rev Neurosci* 6:877–888.
17. Daw NW, Fox K, Sato H, Czepita D (1992) Critical period for monocular deprivation in the cat visual cortex. *J Neurophysiol* 67:197–202.
18. Lehmann K, Löwel S (2008) Age dependent ocular dominance plasticity in adult mice. *PLoS One* 3:e3120.
19. Gall GAE, Kyle WH (1968) Growth of the Laboratory mouse. *Theor Appl Genet* 38:304–308.
20. Kaschube M, et al. (2003) The pattern of ocular dominance columns in cat primary visual cortex: Intra and interindividual variability of column spacing and its dependence on genetic background. *Eur J Neurosci* 18:3251–3266.
21. Kaschube M, Wolf F, Geisel T, Löwel S (2002) Genetic influence on quantitative features of neocortical architecture. *J Neurosci* 22:7206–17.
22. Horton JC, Adams DL The cortical column: A structure without a function. *Philos T R Soc B* 360:837–862.
23. Durbin R, Mitchison G (1990) A dimension reduction framework for understanding cortical maps. *Nature* 343:644–647.
24. Wolf F, Geisel T (1998) Spontaneous pinwheel annihilation during visual develop ment. *Nature* 395:73–78.
25. Goodhill GJ, Cimponeriu A (2000) Analysis of the elastic net model applied to the formation of ocular dominance and orientation columns. *Network-Comp Neural* 11:153–168.
26. Swindale NV (1980) A model for the formation of ocular dominance stripes. *P Roy Soc Lond B Bio* 208:243–264.
27. Miller KD, Keller JB, Stryker MP (1989) Ocular dominance column development: Analysis and simulation. *Science* 245:605–615.
28. Obermayer K, Blasdel G, Schulten K (1992) Statistical mechanical analysis of self organization and pattern formation during the development of visual maps. *Phys Rev A* 45:7568–7589.
29. Newell AC, Whitehead JA (1969) Finite bandwidth, finite amplitude convection. *J Fluid Mech* 38:279–303.
30. Cross MC, Hohenberg PC (1993) Pattern formation outside of equilibrium. *Rev Mod Phys* 65:851–1112.
31. Cross MC, Greenside H (2009) *Pattern Formation and Dynamics in Nonequilibrium Systems* (Cambridge University Press, Cambridge, UK).
32. Chklovskii DB, Schikorski T, Stevens CF (2002) Wiring optimization in cortical circuits. *Neuron* 34(3):341–347.
33. Kang K, Shelley M, Sompolinsky H (2003) Mexican hats and pinwheels in visual cortex. *Proc Natl Acad Sci USA* 100:2848–2853.
34. Swindale NV, Shoham D, Grinvald A, Bonhoeffer T, Hubener M (2000) Visual cortex maps are optimized for uniform coverage. *Nat Neurosci* 3:822–826.
35. Müller T, et al. (2000) An analysis of orientation and ocular dominance patterns in the visual cortex of cats and ferrets. *Neural Comput* 12:2573–2595.
36. Chapman B, Stryker MP, Bonhoeffer T (1996) Development of orientation preference maps in ferret primary visual cortex. *J Neurosci* 16(20):6443–6453.
37. Kaschube M, Schnabel M, Wolf F, Löwel S (2009) Interareal coordination of columnar architectures during visual cortical development. *Proc Natl Acad Sci USA* 106:17205–17210.
38. Oster AM, Bressloff PC (2006) A developmental model of ocular dominance column formation on a growing cortex. *B Math Biol* 68:73–98.
39. Wang BS, Sarnaik R, Cang J (2010) Critical period plasticity matches binocular orientation preference in the visual cortex. *Neuron* 65:246–256.
40. Olson CR, Freeman RD (1980) Profile of the sensitive period for monocular deprivation in kittens. *Exp Brain Res* 39:17–21.
41. Schmidt KF, Löwel S (2006) Optical imaging in cat area 18: Strabismus does not enhance the segregation of ocular dominance domains. *Neuroimage* 29(2):439–445.